

# Gallium enhances reconstructive properties of a calcium phosphate bone biomaterial

Ivana Strazic Geljic<sup>1,2</sup>, Nicolas Melis<sup>1</sup>, Florian Boukhechba<sup>1,2</sup>, Sébastien Schaub<sup>1</sup>, Charlotte Mellier<sup>2</sup>, Pascal Janvier<sup>3</sup>, Jean-Pierre Laugier<sup>4</sup>, Jean-Michel Bouler<sup>3</sup>, Elise Verron<sup>5†</sup> and Jean-Claude Scimeca<sup>1\*†</sup> 

<sup>1</sup>Université Nice Sophia Antipolis, CNRS, Inserm, iBV, Nice, France

<sup>2</sup>GRAFTYS SA, Aix en Provence, France

<sup>3</sup>CNRS, CEISAM, UMR6230, Nantes, France

<sup>4</sup>CCMA, Université Côte d'Azur, BP71, Nice, France

<sup>5</sup>LIOAD, Université de Nantes, Inserm UMR791BP84215, Nantes, France

## Abstract

Calcium phosphate (CaP)-based biomaterials are commonly used in bone reconstructive surgery to replace the damaged tissue, and can also serve as vectors for local drug delivery. Due to its inhibitory action on osteoclasts, the semi-metallic element gallium (Ga) is used for the systemic treatment of disorders associated with accelerated bone resorption. As it was demonstrated that Ga could be incorporated in the structure of CaP biomaterials, we investigated the biological properties of Ga-loaded CaP biomaterials. Culturing bone cells on Ga–CaP, we observed a decrease in osteoclast number and a downregulation of late osteoclastic markers expression, while Ga–CaP upregulated the expression of osteoblastic marker genes involved in the maturation of bone matrix. We next investigated *in vivo* bone reconstructive properties of different Ga-loaded biomaterials using a murine bone defect healing model. All implanted biomaterials showed a good osseointegration into the surrounding host tissue, accompanied by a successful bone ingrowth and bone marrow reconstruction, as evidenced by histological analysis. Moreover, quantitative micro-computed tomography analysis of implants revealed that Ga enhanced total defect filling. Lastly, we took advantage for the first time of a particular mode of non-linear microscopy (second harmonic generation) to quantify *in vivo* bone tissue reconstruction within a CaP bone substitute. By doing so, we showed that Ga exerted a positive impact on mature organized collagen synthesis. As a whole, our data support the hypothesis that Ga represents an attractive additive to CaP biomaterials for bone reconstructive surgery. Copyright © 2017 John Wiley & Sons, Ltd.

Received 9 June 2016; Revised 20 December 2016; Accepted 9 January 2017

**Keywords** bone reconstruction; calcium phosphate cements; gallium; gallium bone delivery; osteoclast/osteoblast crosstalk; second harmonic generation quantitative analysis; bone repair quantification

## Introduction

In the field of bone tissue engineering, major efforts are currently focused on the development of novel biomaterials usable for bone reconstruction. Calcium phosphate (CaP) biomaterials are considered the best alternative to bone grafting because of their biocompatibility and chemical properties suitable for bone remodelling (LeGeros, 1988; Libicher *et al.*, 2006; Ooms *et al.*, 2003a, b; Rush, 2005; Tomita *et al.*, 2003; Welch *et al.*, 2003). Among them, CaP cements (CPCs), based on studies performed originally by LeGeros in 1982 (LeGeros, 1982) and Brown and Chow in 1986 (Brown and Chow, 1986), have considerably revolutionized the world of bone tissue engineering, due to their mouldability, injectability, rapid integration into the bone structure and progressive resorption rate. Different injectable bioresorbable CPCs have been

developed and commercialized for dental and orthopaedic indications in both EU and US markets since 2009.

After implantation into the bone defect, CPCs are able to self-set (Chen *et al.*, 2003) and harden without any significant exothermic reaction that could be prejudicial to the bone tissue and/or loaded drug. Thus, CPC combined devices loaded with active molecules represent good candidates for sustained local drug delivery (Ginebra *et al.*, 2012).

In the early 1970s, it was demonstrated that the semi-metallic element gallium (Ga) had several therapeutic effects [for a review see Chitambar (2010)], including: (i) the inhibition of neoplastic proliferation; (ii) the treatment of some pathogens such as species of *Mycobacterium* (Bernstein, 1998); (iii) the decrease of accelerated bone mineral resorption, which occurs during osteolytic bone diseases, and the subsequent lowering of elevated plasma calcium levels associated with these pathologies. In this context, Ga has been used to treat hypercalcaemia resulting from malignant tumours such as parathyroid carcinoma, and Paget's disease of bone (Warrell *et al.*, 1984, 1990, 1988). This anti-hypercalcaemic effect of Ga results from

\*Correspondence to: J. C. Scimeca, iBV, Institut de Biologie Valrose, Université Nice Sophia Antipolis, Tour Pasteur, UFR Médecine, 28 avenue de Valombrose, 06107 Nice Cedex 2, France. E-mail: scimeca@unice.fr

†Authors contributed equally to the supervision of the study.

an inhibition of bone resorption (Bockman, 2003; Warrell *et al.*, 1984). Indeed, due to its chemical characteristics, Ga presents an affinity for biological apatite, which explains the presence of Ga deposits in bone tissue, and preferentially at sites of rapid bone remodelling, such as active metaphyseal growth plate and healing fractures (Bockman *et al.*, 1986, 1990; Korbas *et al.*, 2004).

Few studies have explored the effect of Ga on bone cells. Hall and Chambers (1990) demonstrated that ionic Ga inhibited bone resorption in a dose-dependent manner and reduced the osteoclastic resorption activity without inducing modifications to the morphology or number of osteoclasts. In contrast to these findings, Blair *et al.* (1992) showed a cytotoxic effect of Ga on osteoclasts. Considering this discrepancy, we previously investigated the biological effect of Ga on bone cells and reported that Ga, administered in cell culture medium, inhibited both the differentiation and the resorbing activity of osteoclasts in a dose-dependent manner (0–100  $\mu\text{M}$ ) without affecting the viability or proliferation of osteoblasts (Verron *et al.*, 2010, 2012b).

Furthermore, studies by Ma *et al.* (2010a, b) on ovariectomized osteopenic rats showed positive effects of orally administered Ga on trabecular bone volume, trabecular and cortical thickness, bone mineral content of the vertebrae and femoral neck strength. Similarly, Stern *et al.* (1994) demonstrated that Ga administration stimulates osteoblast activity in ovariectomy-induced osteopenia associated with a low calcium diet. Nevertheless, this stimulation was not sufficient to prevent osteopenia bone loss in rats. Another study using organic yeast-derived Ga showed that Ga can promote callus bone formation in a fracture healing model in ovariectomized rats (Pei and Fu, 2011). A study in normal rats where Ga was injected intraperitoneally showed lower calcium and vitamin D serum levels, and inhibition of bone resorption, but also bone formation (Wakley *et al.*, 1992). In addition, Jenis *et al.* (1993) found that a subcutaneous 3 week Ga treatment decreased calcium serum levels without any significant effect on bone mineral density in normal rats. The discrepancy in Ga effects on bone in the abovementioned studies could be due to the differences in Ga treatment duration, doses and administration routes, as well as to the fact that some studies used osteoporotic models, whereas others were conducted in rats with normal bone turnover.

Several clinical trials confirmed that Ga was effective against cancer-induced hypercalcaemia resulting from an excessive bone resorption (Collery *et al.*, 2002). Using gallium nitrate alone or combined with other chemotherapeutic agents, significant positive outcomes have been obtained, with patients experiencing recurrence or for patients who responded poorly to conventional chemotherapy (Chitambar, 2012). For example, a small clinical trial involving myeloma patients receiving chemotherapy showed that Ga could attenuate the rate of bone loss (Niesvizky, 2003). As a whole, these data strongly support the therapeutic potential of Ga compounds in the treatment of bone turnover disorders (Verron *et al.*, 2012a).

However, some studies have reported that the systemic administration (oral or parenteral) of Ga compounds results in elevated concentration of Ga in kidneys and liver, possibly generating toxicity issues together with a poor delivery of Ga to the aimed tissue (Verron *et al.*, 2012a). These important drawbacks related to systemic administration could be circumvented by a local Ga delivery. Mellier *et al.* (2011, 2015) have defined suitable protocols for inserting Ga ions into CaP matrices, while generally preserving their textural, mechanical or setting properties. More recently, the same authors assessed the performance of two different types of Ga-loaded CPCs in a rabbit femoral defect model (Mellier *et al.*, 2015) with no significant difference observed 4 weeks after implantation between control and the Ga-containing formulations. The authors underlined that the amount of resorbed biomaterials was quite low, and as a consequence the Ga release, suggesting longer-term implantations in different animal models in order to investigate whether the presence of Ga might improve bone regeneration. With this scope and in the light of our previous findings on the Ga effect on bone cells, when administered in cell culture medium, in the present work we wanted to evaluate the performance of different CaP bone biomaterials as vectors for sustained Ga delivery. For that purpose, we used Ga-loaded CaP pellets as a substrate for bone cell culture and Ga-loaded CaP microparticles for *in vivo* bone tissue reconstruction assays.

## Materials and methods

### Biomaterial synthesis and preparation

Graftys SARL (Aix-en-Provence, France) provided all the biomaterials used in this study. A very detailed account of biomaterial synthesis and their physicochemical characterization is described in Mellier *et al.* (2011, 2015). A short overview of the synthesis and processing of the biomaterials is presented in Figure 1. Briefly, the solid phase of control CPC consisted of  $\alpha$ -tricalcium phosphate ( $\alpha$ -TCP,  $\text{Ca}_3(\text{PO}_4)_2$ , 78 wt.%), dicalcium phosphate anhydrous (DCPA,  $\text{CaHPO}_4$ , 10 wt.%), calcium-deficient apatite (CDA,  $\text{Ca}_{10-x}[\square]_x(\text{HPO}_4)_y(\text{PO}_4)_{6-y}(\text{OH})_{2-z}[\square]_z$ , 10 wt.%) and polymer hydroxypropyl methyl cellulose (HPMC, 2 wt.%). For Ga-loaded CPC (CPC/Ga), the CDA part of the cement powder was loaded with Ga ions by surface adsorption, as previously described in Mellier *et al.* (2011, 2015). Briefly, CDA/Ga was synthesized by co-precipitation from a mixture of gallium nitrate hydrate, calcium nitrate tetrahydrate and diammonium hydrogen phosphate with the (Ca + Ga)/P molar ratio at 1.51 and the Ga/Ca molar ratio in the 0–0.08 range. At the end of synthesis, the white precipitate was dried at 70°C for 24 h. The amount of Ga incorporated in the isolated solid phase was 3 wt.%, as determined by atomic absorption spectroscopy and X-ray

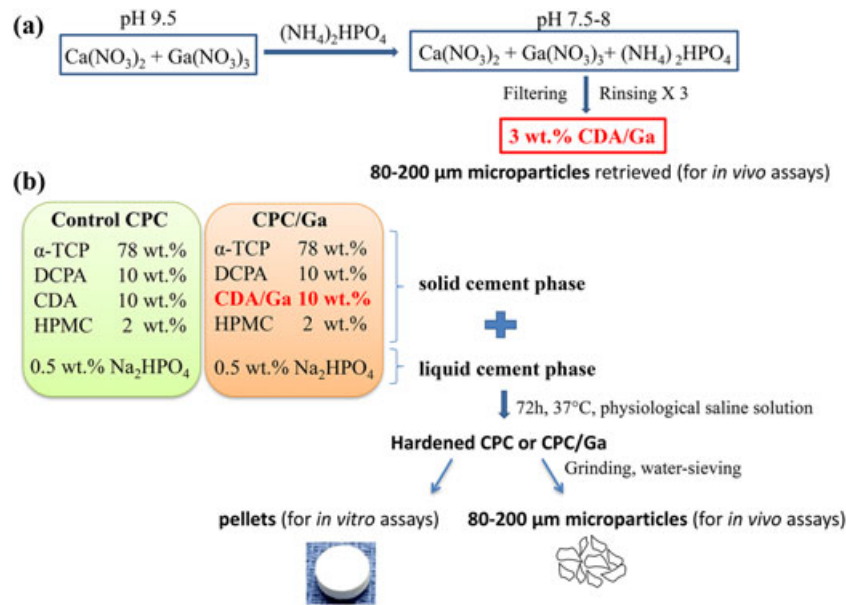


**Figure 1.** Biomaterials synthesis, composition and processing. (A) Brief overview of the direct synthesis of calcium deficient apatite (CDA) under controlled pH conditions (with  $\text{NH}_4\text{OH}$  28 v/v %), loaded with 3 wt.% gallium (Ga). After filtering and extensive rinsing, the product was dried, compacted and ground, and 80–200  $\mu\text{m}$  microparticles were water sieved and implanted into rat bone defect. (B) Composition and physicochemical processing of the cement samples. After 2 min of mixing of the solid and liquid phase, cement has hardened for 72 h at 37°C in physiological saline solution. The obtained samples were either used for cell culture in the form of pellets or ground and water sieved to retrieve 80–200  $\mu\text{m}$  microparticles for *in vivo* implantations. CPC, calcium phosphate cement; CPC/Ga, gallium-loaded CPC;  $\alpha$ -TCP,  $\alpha$ -tricalcium phosphate; DCPA, dicalcium phosphate anhydrous; CDA/Ga, gallium-loaded CDA; HPMC, hydroxypropyl methyl cellulose

diffraction (Mellier *et al.*, 2011). This CDA/Ga comprised 10 wt.% of the solid phase of CPC.

For *in vitro* experiments, the solid powder phase of CPC or CPC/Ga was mixed for 2 min with its liquid phase, consisting of a 0.5 wt.% aqueous solution of  $\text{Na}_2\text{HPO}_4$  (Merck, Darmstadt Germany) in a liquid/solid ratio 0.45  $\text{mlg}^{-1}$ , according to manufacturer's instructions. The obtained paste was placed in silicon moulds and set at 37°C in physiological saline for 72 h. For details on X-ray diffraction patterns and solid-state nuclear magnetic resonance analysis of the biomaterials, please refer to Mellier *et al.* (2011, 2015). Then, solidified pellets with a surface of approximately 0.5  $\text{cm}^2$  were polished and cleaned from dust three times for 15 s in an ultrasound bath. Pellets were further steam sterilized at 121°C for 20 min and incubated for 48 h prior to cell seeding in 1 ml  $\alpha$ -minimal essential medium ( $\alpha$ -MEM) (Sigma-Aldrich, St. Louis USA) supplemented with 10% Hyclone fetal calf serum (FCS; GE Healthcare, Wauwatosa USA), 100 U/ml penicillin (Lonza, Basel Switzerland), 100 U/ml streptomycin (Lonza) and 2% ultraglutamine 1 (Lonza). The medium was replaced three times to neutralize the pH and ion exchange.

For the first set of *in vivo* experiments, already hardened (as described above) CPC or CPC/Ga was ground and water sieved to retrieve microparticles of 80–200  $\mu\text{m}$  in diameter. In the second set of experiments, pure CDA and CDA/Ga were implanted into the rat bone defects. For that purpose, CDA/Ga was prepared as described above and detailed in Mellier *et al.* (2011, 2015). In the end of the physicochemical synthesis, dried precipitates of CDA/Ga were compacted under 150 MPa, ground and water sieved to retrieve microparticles of 80–200  $\mu\text{m}$  in diameter. The control

CDA without Ga was processed in the very same manner.

### Cell culture

Both cell types used in this study, primary human osteoblasts and monocytes, were cultured in  $\alpha$ -MEM medium supplemented with 10% Hyclone FCS, 100 U/ml penicillin, 100 U/ml streptomycin and 2% ultraglutamine 1. For experiments, human primary osteoblasts (#CC-2538, Lonza) were expanded to  $\text{P}_7$  at 6000 cells/ $\text{cm}^2$ . Human primary monocytes were isolated from whole blood samples of healthy individuals (provided by Etablissement Français du Sang La Plaine St Denis, France) using Uni-SepMaxi tubes (NOVAMED Ltd, Jerusalem Israel) and Easy Sep Human Monocyte Enrichment Kit (STEMCELLS Technologies, Vancouver Canada) according to manufacturers' instructions. After seeding freshly isolated monocytes, the differentiation towards osteoclasts was triggered by adding 66 ng/ml receptor activator of nuclear factor kappa-B ligand (RANKL) (Peprotech, Neuilly sur Seine France) and 33 ng/ml macrophage-colony stimulating factor (M-CSF) (Peprotech) simultaneously to the culture medium. After each medium renewal, RANKL and M-CSF were added at the same concentrations as after cell seeding. For co-culture experiments osteoblasts were seeded at 100 000 cells/pellet and 4 hours later (after osteoblastic adhesion), monocytes were added at 200 000 cells/pellet. In co-culture experiments no exogenous ligands were added to the culture medium. Both for monoculture and for co-culture, the culture medium was renewed every third day.

## Cell viability assays

Human primary osteoblasts at P<sub>7</sub> were seeded at 50 000 cells/pellets and freshly isolated human primary monocytes at 90 000 cells/pellet for cell viability assessment in monoculture. For co-culture conditions, 100 000 osteoblasts and 200 000 monocytes/pellet were seeded. At days 3, 6 or 14 of culture, cells were rinsed two times in phosphate-buffered saline (PBS; Lonza) and incubated in 0.5 mg/ml 3-(4,5-dimethylthiazol-2-yl)-2,5-diphenyltetrazolium bromide (MTT; Sigma-Aldrich) for 1 h in a cell incubator. MTT was aspirated delicately and 0.3 ml lysis buffer (sodium dodecyl sulphate 10%, HCl 0.01 N) was added/well and left overnight at room temperature, in the dark. The next morning, supernatants were centrifuged 2 min at 20 000 g and absorbance was measured in 100  $\mu$ l at 562 nm. In parallel experiments, using increasing amounts of cells cultured on plastic or pellets, we verified the relationship between cell number and MTT assay result (data not shown).

## Tartrate-resistant acid phosphatase (ACP5) staining

Human primary monocytes were seeded alone at 200 000 cells/pellet or co-cultured with 100 000 human primary osteoblasts, without the addition of osteoclast differentiation ligands. For negative staining control, 100 000 osteoblasts/pellet were seeded alone. After 7 or 14 days, cells were rinsed two times in PBS and fixed in citrate/acetone solution for 30 s. ACP5<sup>+</sup> cells were revealed using the acid phosphatase, leukocyte kit following the manufacturer's instructions (# 387A; Sigma-Aldrich).

## Gene expression analysis

For monoculture experiments, 100 000 human primary osteoblasts or 200 000 freshly isolated human primary monocytes were seeded on plastic or biomaterial pellets. For co-culture conditions, 100 000 osteoblasts and 200 000 monocytes/pellet were seeded. At days 2, 5, 7 or 14, cells were rinsed two times in PBS and incubated in 0.25 % trypsin/ethylene diamine tetra acetic acid (EDTA; Lonza) at 37°C for 5 min. Total RNA was extracted using the NucleoSpin RNA XS kit (Macherey-Nagel, Duren Germany) following manufacturer's instructions and RNA concentration was measured on Nanodrop 2000 spectrophotometer (Thermo Fisher Scientific, Waltham USA). 150 ng RNA was used as a template for cDNA synthesis using random primers and SuperScript II reverse transcriptase (Invitrogen, Waltham USA) in Flexcycler (Analytik Jena, Jena Germany). Total cDNAs were diluted 10 times and 5  $\mu$ l template was used for quantitative real-time polymerase chain reaction (PCR) assay (StepOne Plus, Life Technologies, Waltham USA). Reactions were performed in a 20  $\mu$ l final volume with quantitative PCR mastermix GoTaq (Promega, Madison USA). Amplification conditions were as follows: 2 min at 50°C, 10 min at 95°C, 40 cycles (15 s at 95°C, 1 min at

60°C). The expression of genes of interest was normalized to ribosomal protein large P0 (*RPLP0*) gene expression, quantified by the comparative 2<sup>-Ct</sup> method and expressed as a fold change compared with control conditions without Ga. The primers used in quantitative real-time PCR are listed in Table 1.

## Field-emission scanning electron microscopy analysis

Human primary osteoblasts and human primary monocytes were mono- or co-cultured as described above. Cells seeded on biomaterial pellets were fixed overnight at 4°C in a buffered glutaraldehyde solution, rinsed, dehydrated in a graded ethanol series, immersed in hexamethyldisilazane (Sigma-Aldrich) for 5 min and dried at room temperature. The samples were then mounted on aluminium stubs and sputter coated with gold-palladium (Cressington, 308R, Watford UK). An examination was performed using a field-emission scanning electron microscope (FESEM JEOL 6700F, Tokyo, Japan).

## Orthotopic implantation of biomaterial microparticles in rat

All animal procedures obtained the approval of the local animal health care committee (CIEPAL NCE/2012-69) and were conducted in accordance with European Community guidelines for the care and use of laboratory animals (Directive 2010/63/UE). Bilateral femoral implantations of biomaterial microparticles were performed on 16 male Lewis rats weighing approximately 300 g (Janvier Labs, Le Genest-Saint-Isle France), in aseptic conditions under general anaesthesia induced by

Table 1. Human primers for quantitative polymerase chain reaction

Gene	Forward primer (5' → 3')	Reverse primer (5' → 3')	GI
<i>ACP5</i>	gaccaccttggcaatgtctctg	tggctgaggaagtcatctgagttg	161377454
<i>ALPL</i>	gtacgagctgaacaggaacaacg	cttggcttttctctcatggtg	294712525
<i>BGLAP</i>	gggtcagccttgggtcaca	ggctcccagccattgatcag	314122170
<i>COL1A1</i>	ctctgacgcacggcc	ccgttctgacgcaggtgatt	110349771
<i>CTSK</i>	tgaggcttcttgggttccatc	aaaggggtcattactgcggg	315075295
<i>FBJ</i>	tgctctcctcaatgacctga	ataggtccatgtctgacagga	254750707
<i>IBSP</i>	ctgtgccactactgctt	caaaatgctgacaaaataaagc	167466186
<i>ITGB3</i>	cattactctgctcactacca	aacggatttcccataagca	47078291
<i>JDP2</i>	cttcttctgttccggcatc	cttctgtaggtgaaactgg	205277420
<i>MCSF</i>	tgacggcgtgattgaca	gatcttcaactgttctggtctaca	166235151
<i>MMP9</i>	ctggagacacctgagaaccaatc	ccaccggagtgaaccatagc	74272286
<i>NFATC1</i>	gcatcacagggaagaccgtgtc	gaagttcaatgtcggagttctgag	27502384
<i>ON</i>	accagcacccttgcagc	agggtcacaggtctcgaataaagc	48675809
<i>OPG</i>	ctctcaagccctgaaaggtt	cctgggtgtccactaatgg	148743792
<i>OPN</i>	agaagtttcgacagactgacatc	gatggcctgtatgcaccatt	91598938
<i>POSTN</i>	tgaaggtggtgatggtcattatt	cgcttcttagactctgaactttttgt	209862910
<i>RANKL</i>	ctcagccttctgctcactcact	ccaagaggacagactcattatgg	197927084
<i>RPLP0</i>	tgatcatgacccattctatcat	aggcagatggatgacccaaga	490871444
<i>RUNX2</i>	gcttctgcatcaccga	tcagtgagggtgaaatgctgtg	226442790

ACP5, acid phosphatase 5 tartrate resistant; ALPL, alkaline phosphatase; BGLAP, bone gamma-carboxyglutamate (Gla) protein (osteocalcin); COL1A1, collagen type I, alpha 1; CTSK, cathepsin K; FBJ, c-Fos; IBSP, integrin-binding sialoprotein; ITGB3, integrin, beta 3; JDP2, jun dimerization protein 2; MCSF, macrophage colony-stimulating factor 1; MMP9, matrix metalloproteinase 9; NFATC1, nuclear factor of activated T-cells cytoplasmic 1; ON, osteonectin; OPG, osteoprotegerin; OPN, osteopontin; POSTN, periostin osteoblast specific factor; RANKL, receptor activator of nuclear factor kappa-B ligand; RPLP0, ribosomal protein large P0; RUNX2, runt-related transcription factor 2.

inhalation of isoflurane 5% and maintained by intramuscular injections of xylazine 10 mg/kg and ketamine 50 mg/kg. The implants were prepared as previously described (Balaguer *et al.*, 2010; Boukhechba *et al.*, 2011). Briefly, in 1 ml syringes (Therumo Europe N.V., Leuven Belgium) 60 mg CPC, CPC/Ga, CDA or CDA/Ga 80–200  $\mu\text{m}$  microparticles (previously heat-sterilized at 180°C for 3 h) were extemporaneously mixed with 100  $\mu\text{l}$  previously prepared rat platelet-poor plasma. The coagulation of plasma was triggered by adding 10  $\mu\text{l}$  2%  $\text{CaCl}_2$ , 2  $\text{H}_2\text{O}$  solution (Merck, Germany) and 1 U thrombin (Sigma-Aldrich). After at least 15 min, the tops of the syringes were cut off and coagulated microparticles were implanted with a spatula in a  $3 \times 2.7$  mm cylindrical defect drilled at the distal epiphyseo-metaphysal junction in rat femora. In the first set of experiments, six animals were implanted with CPC or CPC/Ga contralateral; in the second set, 10 animals were implanted with CDA or CDA/Ga contralateral. After 2 months, animals were sacrificed by inhalation of  $\text{CO}_2$  and the bone specimens were retrieved immediately and stored in 70% ethanol.

### Three-dimensional microtomography analysis

Physiological saline-immersed rat femora were scanned with Skyscan 1172 microtomograph (Bruker, Billerica USA) equipped with 12-bit digital CCD camera. Samples were placed with the axis of the femur perpendicular to the plane of scanning and cross-section images were acquired under 90 kV voltage and 88  $\mu\text{A}$  current with a 1 mm aluminium filter. The rotation step was set at 0.7° and the exposure time per step was 776 ms. Three-dimensional reconstruction of 6  $\mu\text{m}$  resolution cross-section images was carried out in NRecon software (Bruker) using a modified Feldkamp cone-beam algorithm, as provided by the manufacturer. The parameters were set as follows: smoothing at 3, ring artefact correction at 10, beam hardening correction at 50%, rotation angle 180° and image conversion values in 0.003–0.03 ranges. To quantify bone regeneration and biomaterial degradation in the defects, the region of interest was set to the whole implant area excluding the cortical part in CTAn analysis software (Bruker).

### Histological preparation and analysis

CPC and CPC/Ga explants were fixed for 24 h in neutral formalin solution (pH 7.2) and then dehydrated in baths with ethanol concentration increasing from 70% up to 100% for 3 days/bath. Bone specimens were then infiltrated and embedded in methyl methacrylate, as previously described (Verron *et al.*, 2010). Undecalcified serial 5  $\mu\text{m}$  sections were cut using a hard tissue microtome (Supercut 2050, Reichert-Jung, Depew, USA) equipped with a D profile tungsten carbide knife. These sections were stained with haematoxylin/eosin (HE) and assessed to visualize mature bone, osteoid tissue, bone marrow and residues of biomaterial microparticles. CDA

and CDA/Ga explants were fixed for 24 h in neutral formalin solution (pH 7.2) and then decalcified in 10% EDTA (pH 8) for 4 weeks. These samples were embedded in paraffin and 5  $\mu\text{m}$  thick sections were prepared and stained with HES to visualize the relevant bone structures and biomaterial microparticles. All histological sections were imaged by Nikon Eclipse 80i (Nikon, Tokyo, Japan) for qualitative observations.

### Second harmonic generation (SHG) preparation and analysis

SHG microscopy relies on a highly specific optical phenomenon produced in a very limited number of biological structures (type I collagen fibres, myosin II fibres and tubulin) (Vielreicher *et al.*, 2013). Imaging type I collagen by SHG microscopy requires excitation laser wavelengths from 720 to 960 nm, while the generated SHG signal is exactly half of the excitation wavelength. For bone tissue, SHG microscopy's ability to detect predominantly organized collagen fibres has been experimentally validated by several comparative studies using techniques such as immunofluorescence staining light microscopy, polarized light microscopy and scanning electron microscopy (Ambekar *et al.*, 2012). As SHG has intrinsic specificity for collagen fibres, this results in high contrast images, with no additional staining needed. Thus, tissue sections prepared (as described above) for histological study were also used for SHG imaging (Zeiss LSM 710 microscope, Oberkochen Germany). The Mai Tai laser excitation wavelength was set to 880 nm and the SHG signal was detected in transmission and reflection mode. For CPC and CPC/Ga, 5  $\mu\text{m}$  sections were qualitatively analysed; for CDA and CDA/Ga explants, additional 100  $\mu\text{m}$  sections were cut to carry out quantification on a larger portion of the samples. Quantitative comparison of collagen signal between Ga and control samples was performed on the whole implant area using an in-house quantification tool developed in Matlab programming language by S. Schaub from iBV PRISM platform (Platform of Resources in Imaging and Scientific Microscopy).

### Statistical analysis

*In vitro* results are expressed as a mean  $\pm$  standard deviation of three independent experiments each performed in triplicate. Differences between Ga and the control group were evaluated by a bidirectional Mann and Whitney U test with the risk threshold set at 5%. For microtomography experiments, significant differences in total defect filling between Ga and control groups were determined by bidirectional Kruskal-Wallis one-way analysis of variance with the risk threshold set at 5%. For SHG quantitative analysis, a bidirectional Mann and Whitney U test with the risk threshold set at 5% was

used to assess significant differences between Ga and control biomaterials.

## Results

### Human primary bone cells culture on apatitic matrices loaded with Ga

Human primary monocytes were seeded on CPC or CPC/Ga pellets and cultured for 3 or 6 days before an MTT assay was performed. In parallel experiments (data not shown), we verified that MTT assay results correlated with the number of viable cells seeded on apatitic

matrices. As shown in Figure 2A, and compared with the CPC control condition, seeding monocytes on CPC/Ga resulted in slightly decreased cell viability/number for both time points. We also performed a cell structure examination using scanning electron microscopy analysis. As depicted in Figure 2B, we observed monocytes on CPC and CPC/Ga (white arrowheads), as well as cellular extensions interacting with the cement surface. In the presence of the osteoclastogenic agent RANKL, few cells exhibiting osteoclast-like morphology were also observed. However, these events remained rare for both cements. Lastly, we performed quantitative real-time PCR experiments to quantify the expression of early and late osteoclastogenesis marker genes (gene symbols are

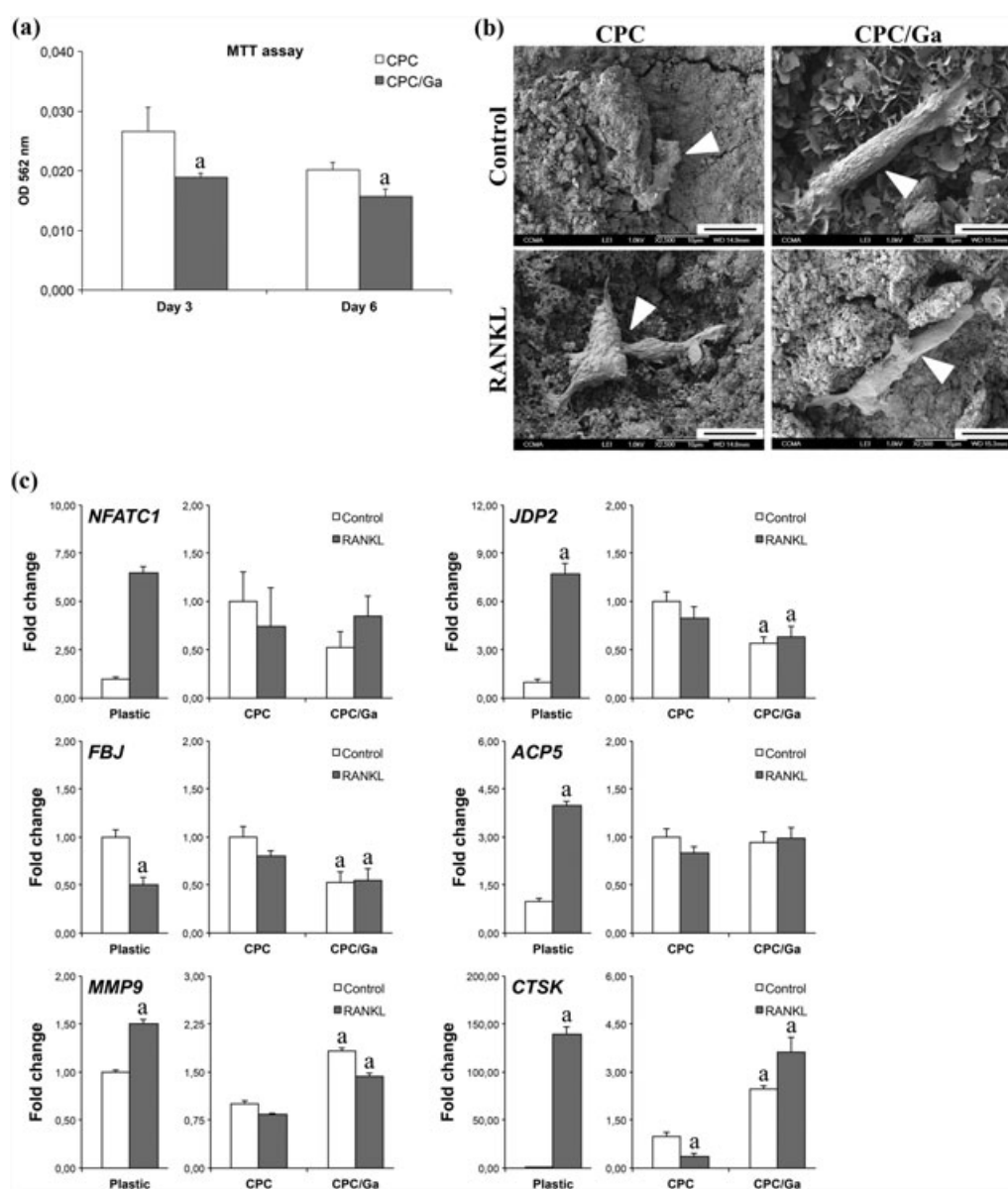


Figure 2. Cellular proliferation, morphology and differentiation of human primary monocytes on calcium phosphate cement (CPC) or gallium-loaded CPC (CPC/Ga) pellets. (A) 3-(4,5-dimethylthiazol-2-yl)-2,5-diphenyltetrazolium bromide (MTT) assay: 90 000 monocytes were cultured for 3 or 6 days. Data represent the mean  $\pm$  standard deviation of three independent experiments, with each including five MTT measures. (B) Field-emission scanning electron microscopy analysis of pellets seeded with monocytes and cultured for 5 days in the presence of hM-CSF (33 ng/ml; upper panels) or in the presence of hM-CSF/hRANKL (33 ng/ml and 66 ng/ml, respectively; lower panels). The white arrowheads indicate cells (magnification 2500 $\times$ , scale bars: 10  $\mu$ m). (C) Real-time polymerase chain reaction (PCR) quantification of osteoclastogenesis markers. Monocytes were cultured for 2 days (*NFATC1*, *JDP2*) or 5 days (*ACP5*, *MMP9*, *CTSK*), in the presence of 33 ng/ml hM-CSF (control) or 33 ng/ml hM-CSF and 66 ng/ml hRANKL (RANKL). Data represent the mean  $\pm$  standard deviation of three independent experiments, each performed in triplicate. Data were normalized with respect to gene expression on plastic/control or on CPC/control for cell culture on cement pellets. a: statistically significant compared with plastic/control or CPC/control ( $p < 0.05$ , bi-directional analysis)

defined in the Materials and methods section). As shown in Figure 1C, RANKL induced the differentiation of monocytes seeded on plastic, as attested by the expression of early (*NFATC1*, *JDP2*) and late (*ACP5*, *MMP9*, *CTSK*) marker genes. By contrast, RANKL failed to induce any osteoclastic differentiation of monocytes seeded either on CPC or CPC/Ga. We also observed that, whatever the condition (control or RANKL), the expression of the transcription factors *JDP2* and *FBJ* was diminished on CPC/Ga, whereas the late marker genes *MMP9* and *CTSK* were induced in the presence of Ga. This first set of experiments indicated that human primary monocytes did not efficiently differentiate into osteoclasts when seeded alone on CPC or CPC/Ga.

We next seeded human primary osteoblasts on CPC or CPC/Ga and quantified cell viability/number. As shown in Figure 3A, after 3 days of culture, the presence of Ga induced a 40% inhibition of cell viability/number. At day 7, cellular proliferation was observed on both cements, whereas the inhibition observed in the presence of Ga tended to decline (30% instead of 40%). Cell structure

was also examined using scanning electron microscopy analysis. As shown in Figure 3B, osteoblastic morphology remained unchanged when cells were cultured on CPC/Ga compared with control CPC. Lastly, we used quantitative real-time PCR experiments to quantify the expression of osteoblast marker genes (gene symbols are defined in the Materials and methods section) and three kinds of situation were observed (Figure 3C). Firstly, *RUNX2*, *ALPL* and *OPN* were expressed at similar levels at both times on the control cement. Considering the CPC/Ga, the expression of these three genes was inhibited at day 3, and this inhibition tended to decrease at day 7. Second, *BGLAP* expression increased between day 3 and day 7, and no difference was observed comparing CPC and CPC/Ga. Third, *COL1A1*, *IBSP*, *ON* and *POSTN* expression was identical on CPC or CPC/Ga at day 3. At day 7, the expression level of the four genes decreased on both cements (except for *POSTN* gene on CPC/Ga) but remained at higher levels on CPC/Ga compared with control CPC. Taken together, these data indicated that following 7 days of primary osteoblast culture on

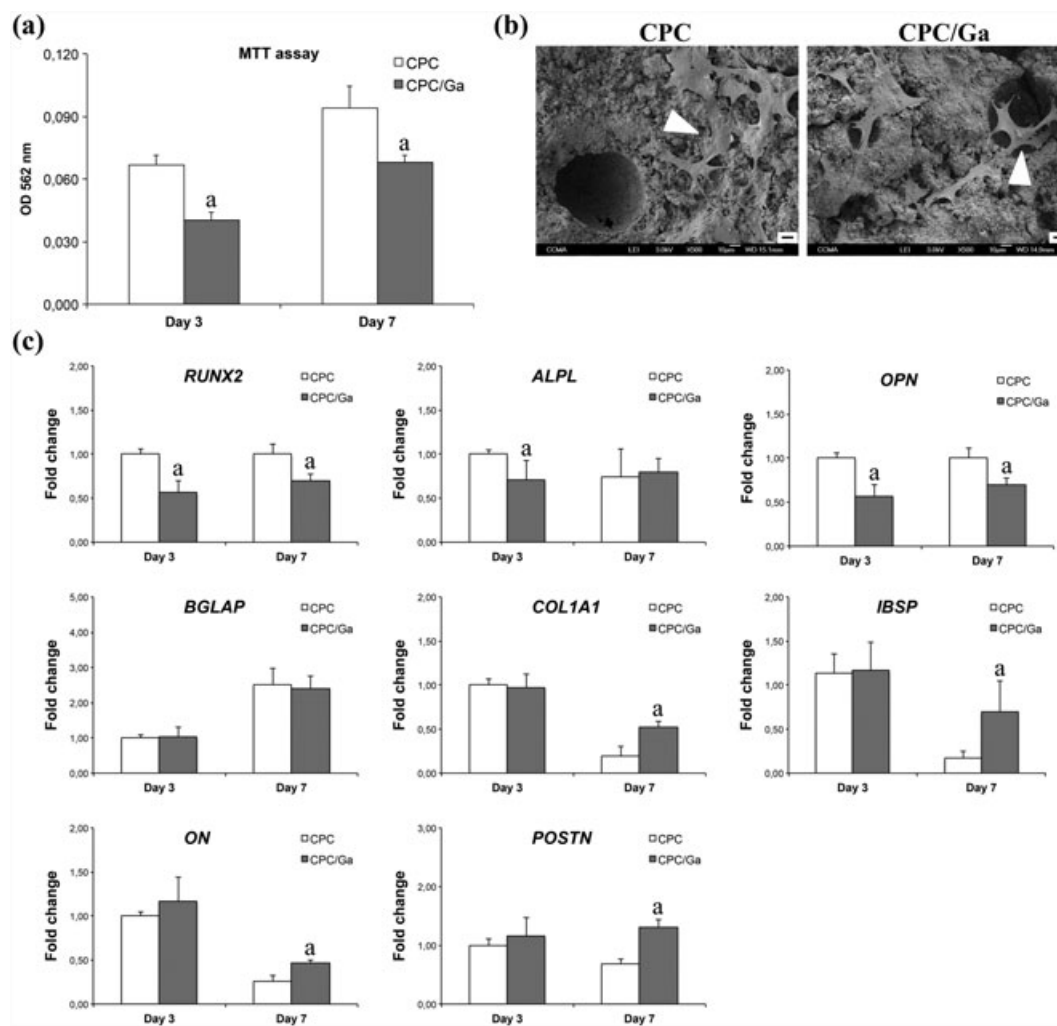


Figure 3. Cellular proliferation, morphology and differentiation of human primary osteoblasts on calcium phosphate cement (CPC) or gallium-loaded CPC (CPC/Ga) pellets. (A) 3-(4,5-dimethylthiazol-2-yl)-2,5-diphenyltetrazolium bromide (MTT) assay: 50 000 osteoblasts were cultured for 3 or 6 days. Data represent the mean  $\pm$  standard deviation of three independent experiments, with each including five MTT measures. (B) Field-emission scanning electron microscopy analysis of osteoblasts cultured for 5 days on pellets. The white arrowheads indicate cells (magnification 500 $\times$ , scale bars: 10  $\mu$ m). (C) Real-time polymerase chain reaction (PCR) quantification of osteoblastic markers after 3 or 7 days of cell culture. Data represent the mean  $\pm$  standard deviation of three independent experiments, each performed in triplicate. Data were normalized with respect to gene expression on CPC at day 3. a: statistically significant compared with CPC/day 3 ( $p < 0.05$ , bi-directional analysis)

cements, the expression level slightly diminished on CPC/Ga for *RUNX2* and *OPN*, was identical for *ALPL* and *BGLAP* and was enhanced on CPC/Ga for *COL1A1*, *ISBP*, *ON* and *POSTN*.

To document monocyte/osteoblast interactions, human primary osteoblasts and human primary monocytes were

then co-cultured up to 14 days on both cements, in the absence of any additional effectors such as M-CSF and RANKL. As depicted in Figure 4A, cell viability/number decreased between day 3 and day 7, and in a lesser extent between day 7 and day 14. Except for day 3, no difference was observed between the two cements. Regarding cellular

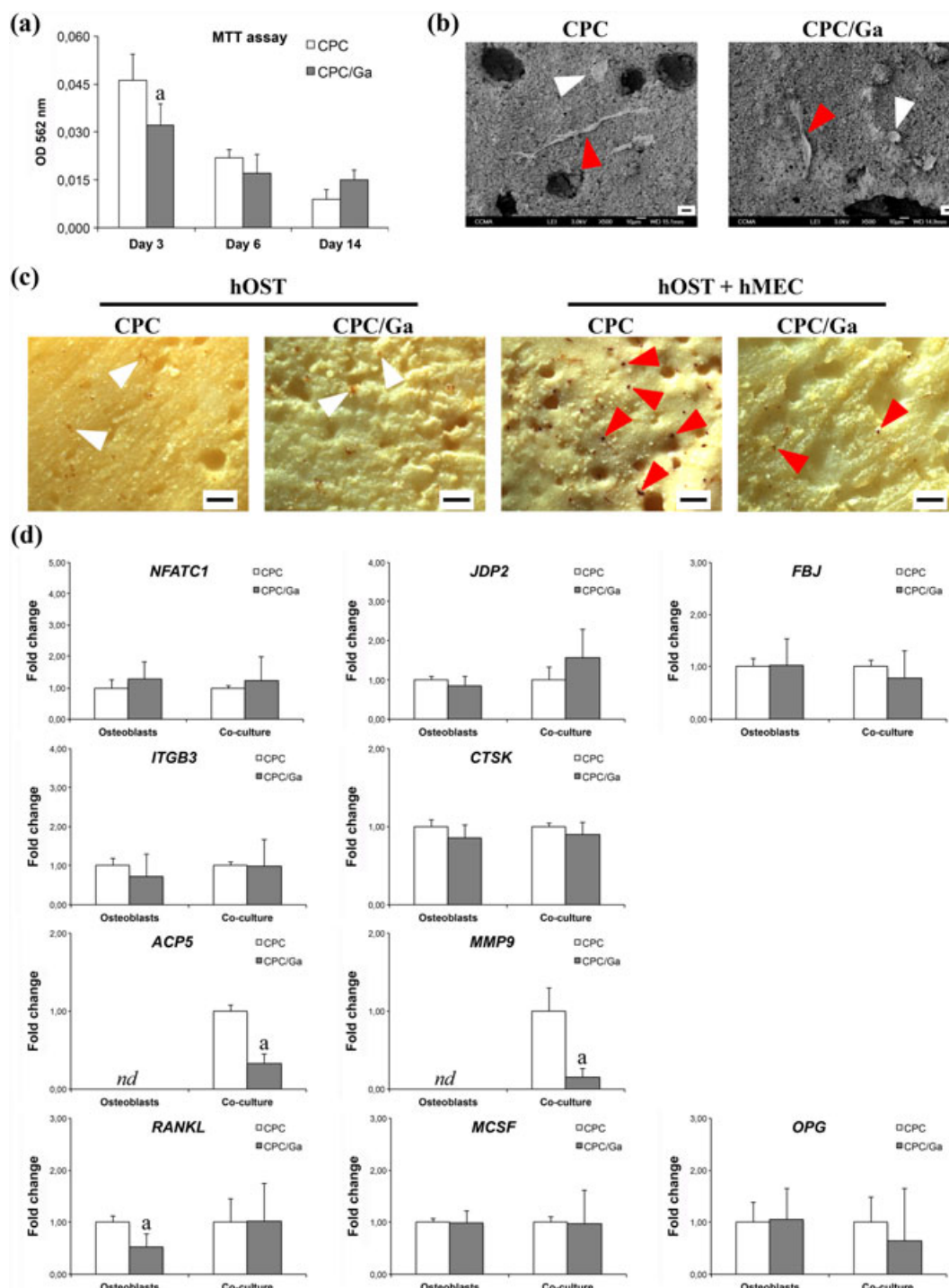


Figure 4. Cellular proliferation, morphology and differentiation of human primary monocytes co-cultured with human primary osteoblasts on calcium phosphate cement (CPC) or gallium-loaded CPC (CPC/Ga) pellets. (A) 3-(4,5-dimethylthiazol-2-yl)-2,5-diphenyltetrazolium bromide (MTT) assay: 100 000 osteoblasts and 200 000 monocytes were co-cultured for 3, 6 or 14 days. Data represent the mean  $\pm$  standard deviation of three independent experiments, with each including five MTT measures. (B) Field-emission scanning electron microscopy analysis of osteoblasts and monocytes co-cultured for 14 days on pellets. The white and red arrowheads indicate osteoblasts and monocytes, respectively (magnification 500 $\times$ , scale bars: 10  $\mu$ m). (C) Histochemical staining of differentiated monocytes positive (red arrowheads) for ACP5 activity. 100 000 osteoblasts were cultured alone or in the presence of 200 000 monocytes for 14 days (scale bars: 100  $\mu$ m). (D) Real-time polymerase chain reaction (PCR) quantification of osteoclastic markers after 6 or 14 days of osteoblast culture or osteoblasts/monocytes co-culture. Data represent the mean  $\pm$  standard deviation of three independent experiments, each performed in triplicate. For each condition (osteoblasts or co-culture) data were normalized with respect to gene expression on CPC. a: statistically significant compared with CPC ( $p < 0.05$ , bi-directional analysis)

morphology (Figure 4B), we observed osteoblasts on both surfaces (white arrowheads), as well as monocytes differentiating into osteoclasts (red arrowheads). We next performed a histochemical demonstration of ACP5 (also known as TRAP) activity. As shown in Figure 4C (left panels), osteoblasts were stained in yellow/brown (white arrowheads) and no difference was observed on CPC/Ga compared with CPC. Regarding osteoblasts/monocyte co-culture, a purple staining was observed within osteoclasts (right panels, red arrowheads) on both cements, but the number of differentiated cells was decreased on CPC/Ga compared with CPC. To further document this inhibition at the molecular level, we eventually performed quantitative real-time PCR experiments (gene symbols are defined in the Materials and methods section) using RNAs prepared from osteoblasts alone or from osteoblasts co-cultured with monocytes (Figure 4D). Concerning the transcription factors involved in the early steps of osteoclastogenesis, we observed that *NFATC1*, *JDP2* and *FBJ* were expressed in both conditions (osteoblasts alone vs. co-culture), with no significant differences between CPC and CPC/Ga. The same situation was observed for the late marker genes of osteoclastic differentiation, *ITGB3* and *CTSK*. By contrast, the late marker genes *ACP5* and *MMP9* were detected only in co-culture conditions and not in osteoblast alone conditions, suggesting an expression restricted to monocytes differentiated into osteoclasts. In this co-culture situation, *ACP5* and *MMP9* expression was strongly inhibited on CPC/Ga compared with CPC. Lastly, we also tested the expression of *RANKL*,

*MCSF* and *OPG*, the triad of osteoblastic genes regulating osteoclastic differentiation. Considering the co-culture condition, we showed that no difference could be observed between CPC and CPC/Ga. In conclusion, we observed that ACP5 activity histochemical staining revealed an inhibition of osteoclastic differentiation on CPC/Ga compared with CPC. Moreover, this inhibition could also be quantified by quantitative real-time PCR experiments measuring the expression of marker genes restricted to differentiated osteoclasts, i.e. *ACP5* and *MMP9*.

#### Orthotopic *in vivo* implantation of apatitic matrices loaded with Ga

We next performed *in vivo* implantation experiments to determine Ga impact on the reconstructive properties of the CPC under study. As illustrated in Figure 5A, cements were first processed into 80–200  $\mu\text{m}$  diameter microparticles and then implanted within cylinder defects generated in the distal part of rat femurs. After 2 months, implants were retrieved and processed to perform HE staining and SHG analysis on tissue sections, as well as micro-computed tomography quantification of the whole implants. Both HE staining (Figure 5B) and SHG (Figure 5C) methods demonstrated for CPC and CPC/Ga a successful bone reconstruction including newly formed tissue up to the central part of implants and a complete cortical bone restoration, without any inflammatory response or fibrous encapsulation. Based on image

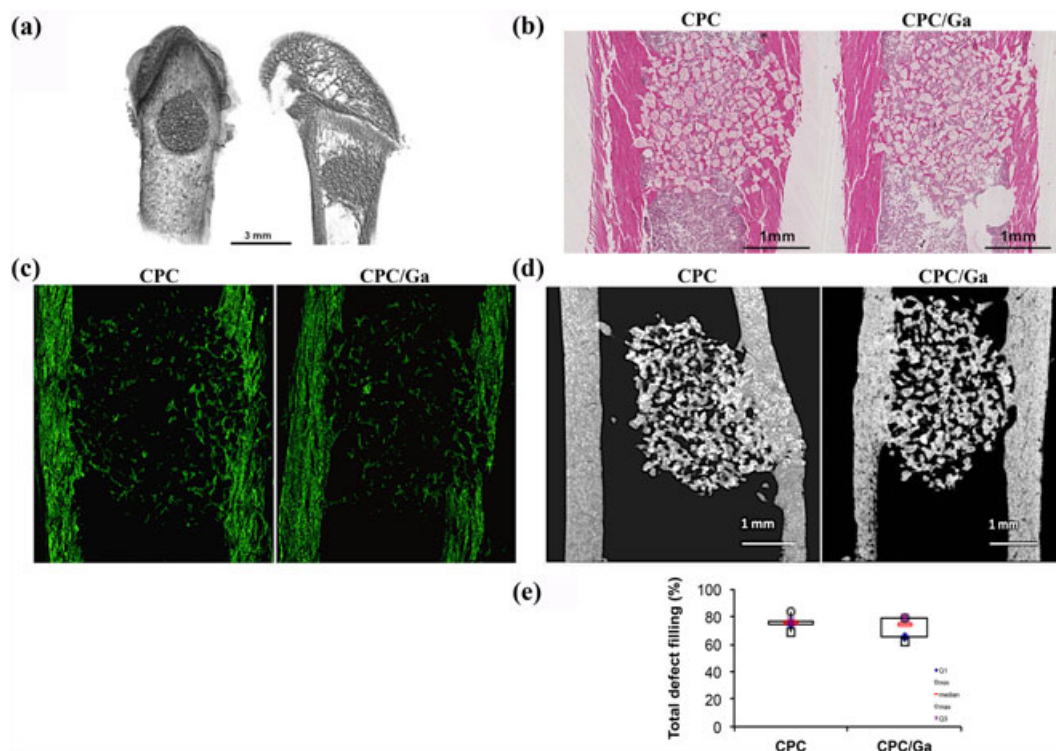


Figure 5. Femoral implantation in rat of calcium phosphate cement (CPC) or gallium-loaded CPC (CPC/Ga) 2 months after implantation. (A) Qualitative three-dimensional micro-computed tomography; (B) HE histological staining; (C) second harmonic generation analysis; (D) quantitative three-dimensional micro-computed tomography analysis; (E) total defect filling quantification: results are expressed as total defect filling rate (CPC,  $n = 6$ ; CPC/Ga,  $n = 6$ )

acquisitions illustrated in Figure 5D, micro-computed tomography was used to quantify total defect filling. The results presented in Figure 5E did not show any significant impact of Ga on bone reconstruction.

With a view to increase Ga content in biomaterial used for bone defects filling, we shifted from CPC to CDA loaded or not with Ga. Indeed, as detailed in the Materials and methods section, Ga was brought to CPC through the CDA part (10%) of the cement solid phase formulation. Thus, using pure CDA allowed increasing Ga content by a factor of 10. As illustrated by HE staining and SHG analysis (Figure 6A, B), and similarly to CPCs, CDA and CDA/Ga implantations led after 2 months to good osseointegration into the surrounding host tissue, accompanied by a successful bone ingrowth and bone marrow reconstruction on the border of the implants. Taking advantage of the unique ability of SHG to specifically detect fibrillar collagen in bone tissue and to carry out quantification on larger implant volumes, we performed 100  $\mu\text{m}$  sections (compared with classical

5  $\mu\text{m}$  histological sections). As shown in Figure 6B (right panel), we measured a 74% increased SHG signal mean intensity with CDA/Ga. These data indicated that higher amounts of fibrillar collagen were synthesized when the reconstruction occurred in the presence of Ga. Lastly, three-dimensional micro-computed tomography was used to quantify total defect filling (Figure 6C). We found that Ga induced a significant 23% increase in defect filling (53.51% vs. 76.89%). Taken together, our results indicated that the Ga presence within CDA used for bone defect filling led to a significantly enhanced bone reconstruction.

## Discussion

*In vitro*, using CPC and CPC/Ga as growing surfaces, primary human monocytes do not differentiate into osteoclasts when cultured in the presence of M-CSF/

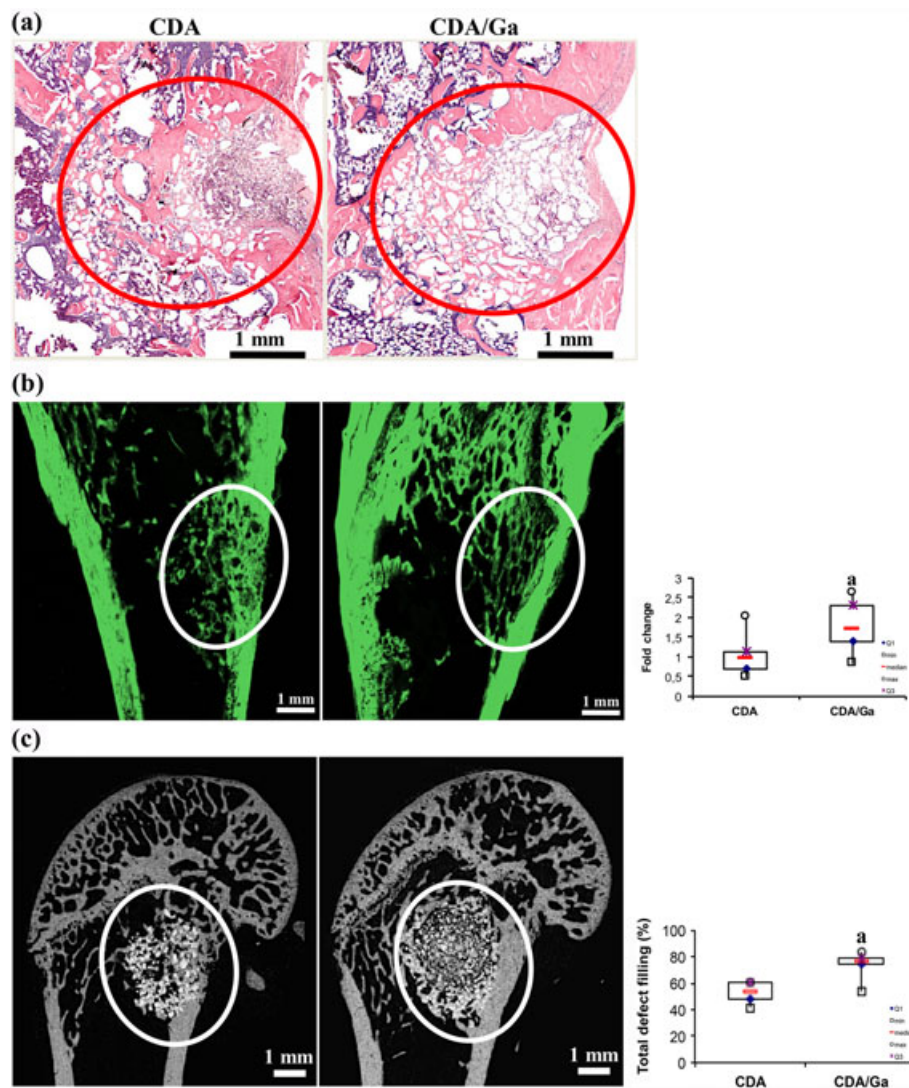


Figure 6. Femoral implantation in rat of calcium phosphate cement (CPC) or gallium-loaded CPC (CPC/Ga) 2 months after implantation. (A) HE histological staining; (B) second harmonic generation (SHG) sections and fibrillar collagen quantification (right panel). Data are normalized with respect to mean SHG intensity per pixel in calcium-deficient apatite (CDA) condition (CDA,  $n = 10$ ; CDA/Ga,  $n = 8$ ). (C) Quantitative three-dimensional micro-computed tomography analysis. Total defect filling quantification: results are expressed as total defect filling rate (CDA,  $n = 9$ ; CDA/Ga,  $n = 10$ ). Red or white circles point to implant area. a: statistically significant compared with CDA ( $p < 0.05$ , bi-directional analysis)

RANKL, whereas successful differentiation was achieved on a plastic surface. Thus, we conclude that the monoculture of primary human monocytes on CPC and CPC/Ga pellets is not a suitable model to study the possible impact of Ga on osteoclastogenesis *in vitro*. In a previous publication, characterizing the properties of cements used in the present study, an increase in the Ga release was observed over time in the presence of RAW264.7 cells seeded on the surface of cement pellets and stimulated with 20 nM RANKL (Mellier *et al.*, 2015). It should be noted that, compared with the human primary cells used for the present study, RAW264.7 is a mouse cell line that required only the presence of RANKL to differentiate into osteoclasts. We can hypothesize that human primary monocytes are more demanding in terms of environment to initiate osteoclastic differentiation. Indeed, in the absence of any exogenous effectors, co-culture with human primary osteoblasts is required to provide all necessary triggers for successful osteoclastogenesis. In these conditions, optimal interactions occurred through a cell-to-cell contact mediated at least by RANKL attached at the surface of osteoblasts and RANK that is expressed at the surface of osteoclasts (Walsh and Choi, 2014).

In co-culture experiments, it is difficult to comment on the Ga impact on marker genes whose expression was also found in osteoblasts alone. Osteoblastic expression has been reported for transcription factors NFATC1 and AP1 family members (Fos/Jun) (Koga *et al.*, 2005; Komori, 2006), as well as for ITGB3 and CTSK (Grzesik and Robey, 1994; Mandelin *et al.*, 2006). However, regarding genes restricted to osteoclasts such as *ACP5* (also known as TRAP) and *MMP9*, Ga exerts an unambiguous and pronounced inhibitory action. Interestingly, Ga impact on *ACP5* expression was further supported at the protein level, as attested by *ACP5* histochemical staining presented in Figure 4. Lastly, we did not observe any Ga-induced variation in *RANKL*, *MCSF* or *OPG* gene expression, suggesting that the Ga inhibition of osteoclasts is not mediated through a modulation of the RANKL/OPG ratio.

When it comes to bone-forming osteoblasts, although we observed *in vitro* a decrease in human primary osteoblasts viability/number on CPC/Ga compared with the control, we evidenced *in vivo* in a rat femoral defect a 23% (total defect filling) and a 74% (fibrillar collagen) positive impact on bone tissue reconstruction. This can be linked to the dual effect Ga exerts, i.e. a decrease in osteoclastogenesis together with an increased osteoblastic production of factors favouring bone construction. In one previous study, using the murine MC3T3-E1 osteoblast precursor cell line, we showed that Ga treatment enhanced the expression of marker genes including alkaline phosphatase (*Alpl*), osterix (*Osx*) and runt-related transcription factor 2 (*Runx2*) (Verron *et al.*, 2010b), thus promoting osteoblastogenesis. In the present study, however, mature differentiated human primary osteoblasts were used and we observed that Ga downregulates the expression of early osteoblastogenic marker *RUNX2*, whereas the expression of alkaline phosphatase (*ALPL*), a by-product of osteoblast activity, remains intact at day 7 of cell culture. On the other

hand, Ga stimulated *COL1A1* expression, which importantly contributes to new tissue formation as the most abundant bone extracellular matrix protein (Gelse *et al.*, 2003). Similarly, Bockman *et al.* (1993) reported that Ga increased type I collagen and fibronectin mRNA, as well as collagen protein levels in primary cultures of rat calvarial osteoblasts. The same year, Jenis *et al.* (1993) published results indicating that Ga increased basal type I collagen mRNA levels and reduced basal osteocalcin mRNA levels in normal rat osteoblasts *in vitro*. We also observed that the expression of genes encoding for non-collagenous proteins was enhanced, including *IBSP*, *ON* and *POSTN*. Bone sialoprotein II (IBSP or BSP II) is a phosphorylated glycoprotein that is involved in the initial steps of bone tissue mineralization (Bouleftour *et al.*, 2014; Chen *et al.*, 1992). Osteonectin (ON; or SPARC for 'secreted protein, acidic and rich in cysteine') is also linked to tissue mineralization along development, remodelling and bone repair (Ribeiro *et al.*, 2014). Regarding periostin (POSTN, originally known as 'osteoblast-specific factor' or OSF2), this glutamate-containing protein is preferentially located in the periosteum, and its expression is enhanced during bone fracture repair (Merle and Garnero, 2012). The abovementioned non-collagenous proteins are mainly expressed in the bone matrix mineralization phase, thus they characterize mature active osteoblasts. Finally, Ga downregulated the expression of osteopontin (*OPN*), a calcium-binding protein that participates in the regulation of mineral crystal growth but also in anchoring osteoclasts to the bone matrix (Liu *et al.*, 2015) and in the formation of their ruffled resorptive borders (Franzen *et al.*, 2008). In addition to the well-described Ga inhibitory action on osteoclastogenesis, our data support the hypothesis that Ga-induced enhancement of bone repair measured *in vivo* could also be linked to an enhancement of the expression of mature osteoblast genes involved in bone tissue formation.

In a cylindrical femoral defect, Ga delivered via CPC failed to show any impact on bone reconstruction within the defect. This is probably due to the low Ga quantities released from the apatite matrix and available in the surrounding tissue. On the contrary, using CDA we demonstrated that the presence of Ga induced a significant stimulation of bone reconstruction, as attested by two types of quantification, i.e. three-dimensional micro-computed tomography scan and SHG analysis. In 1993, Jenis *et al.* reported that systemic Ga administration decreased serum calcium levels and reduced osteocalcin steady-state mRNA levels, while having no effect on type I collagen mRNA levels or bone mineral density *in vivo*. The comparison with these results from Jenis *et al.* (1993) points out how crucial the delivery mode of a pharmacological agent can be. Indeed, using systemic administration of a therapeutic dosage used for the treatment of Paget's disease, they did not observe any impact on bone mineral density of the left femur in normal rats treated with Ga, whereas we measured a positive effect via Ga-loaded biomaterial microparticle implantation. This discrepancy could be related to the

local delivery mode of Ga we used, leading to higher local concentrations of an active molecule released continuously. In addition, and these hypotheses are not exclusive, Jenis *et al.* (1993) reported a Ga effect on normal bone remodelling, whereas we addressed the issue of bone reconstruction following the creation of a defect. Thus, these different physiological situations could also account for our respective observations.

Regarding SHG, these results are in agreement with the data we obtained measuring *COL1A1* gene expression. Actually, SHG analysis allows the quantification of fibrillar collagen (Figure 6B) and we also observed that Ga stimulated *COL1A1* gene expression in primary osteoblasts (Figure 3C). Together, these data reinforce the correlation between molecular data we obtained *in vitro* and bone reconstruction we measured *in vivo*. Importantly, it should be stressed that to our knowledge, this is the first time that the use of SHG is reported in the field of bone reconstruction quantification within a bone substitute implanted *in vivo*. Indeed, concerning osteo-articular applications, SHG analysis has been used to evaluate osteogenic cell differentiation *in vitro* (Brackmann *et al.*, 2012; Flausse *et al.*, 2013; Hronik-Tupaj *et al.*, 2011; Lee *et al.*, 2006; Liskova *et al.*, 2015) or to study tissue samples retrieved from normal or pathological situations (Adur *et al.*, 2013; Ambekar *et al.*, 2012; Caetano-Lopes *et al.*, 2009, 2010; Huang *et al.*, 2015; Masago *et al.*, 2012; Nadiarykh *et al.*, 2007; Paietta *et al.*, 2013; Reiser *et al.*, 2007; Tang *et al.*, 2015). Based on the consistency we observe with gene expression and three-dimensional micro-computed tomography scan quantification data, we demonstrate in the present report that SHG analysis is also fully suitable to monitor the reconstructive properties of a bone substitute upon its implantation *in vivo*.

In conclusion, we propose that the Ga positive impact reported in this study is linked to a decreased osteoclastic differentiation coupled with an increased new bone tissue formation. In terms of mechanisms, this is understated by *in vitro* data obtained at the molecular level through gene expression analysis. *In vivo*, Ga enhanced CaP-induced bone reconstruction, as observed using CDA/Ga to fill bone defects generated in a rat model. Thus, we suggest that the presence of Ga could be beneficial to the process

of bone regeneration, especially in pathological situations related to excessive bone resorption. As a future development, it will be interesting to assess Ga-loaded biomaterial performance in the context of osteoporotic bone. Due to their mechanical properties and *in vivo* resorption rates, we consider that CaP bone substitutes constitute attractive vectors for local Ga delivery to bone.

Interestingly, in addition to the positive impact on bone formation reported here, Ga offers other worthwhile prospects. Indeed, as mentioned in the Introduction section above, Ga displays anti-neoplastic, anti-infectious and anti-inflammatory properties (Chitambar, 2010). Further studies are required to fully evaluate the potentialities of Ga-loaded bone substitutes used for the filling of bone defects for which tumour development and infections represent critical issues.

Finally, as a beneficial side-effect of our quantification experiments, we provide strong data supporting the use of the SHG technique to address the issue of *in vivo* tissue reconstruction within a bone substitute.

## Conflict of interest

Ivana Strazic Geljic, Florian Boukhechba, Charlotte Mellier, Pascal Janvier, Jean-Michel Bouler, Elise Verron and Jean-Claude Scimeca received research support from Graftys SA. The terms of these arrangements have been reviewed and approved by CNRS, the University of Nice Sophia Antipolis and the University of Nantes, in accordance with their policy on objectivity in research.

## Acknowledgements

Nice University, CNRS, Graftys SA (Aix-en-Provence, France) and INSERM supported this work. Julie Lesoeur, Maeva Dutilleul, Paul Pilet, Xavier Mouska, Emilie Goguet-Surmenian, Samah Rekima and Patricia Lagadec are acknowledged for biomaterial implantations and implant analysis after retrieval. The authors gratefully acknowledge iBV PRISM (Platform of Resources in Imaging and Scientific Microscopy) and histopathology platforms, and IRCAN animal core facility. This work was sponsored by Graftys SA, Convention CIFRE N°2011/1356.

## References

- Adur J, Pedroni MV, Steiner CE, *et al.* 2013; The severity of osteogenesis imperfecta and type I collagen pattern in human skin as determined by nonlinear microscopy: proof of principle of a diagnostic method. *PLoS One* **8**: e69186.
- Ambekar R, Chittenden M, Jasiuk I, *et al.* 2012; Quantitative second-harmonic generation microscopy for imaging porcine cortical bone: comparison to SEM and its potential to investigate age-related changes. *Bone* **50**: 643–650.
- Balaguer T, Boukhechba F, Clave A, *et al.* 2010; Biphasic calcium phosphate microparticles for bone formation: benefits of combination with blood clot. *Tissue Eng Part A* **16**: 3495–3505.
- Bernstein LR. 1998; Mechanisms of therapeutic activity for gallium. *Pharmacol Rev* **50**: 665–682.
- Blair HC, Teitelbaum SL, Tan HL, *et al.* 1992; Reversible inhibition of osteoclastic activity by bone-bound gallium (III). *J Cell Biochem* **48**: 401–410.
- Bockman R. 2003; The effects of gallium nitrate on bone resorption. *Semin Oncol* **30**: 5–12.
- Bockman RS, Boskey AL, Blumenthal NC, *et al.* 1986; Gallium increases bone calcium and crystallite perfection of hydroxyapatite. *Calcif Tissue Int* **39**: 376–381.
- Bockman RS, Guidon PT Jr, Pan LC *et al.* 1993; Gallium nitrate increases type I collagen and fibronectin mRNA and collagen protein levels in bone and fibroblast cells. *J Cell Biochem* **52**: 396–403.
- Bockman RS, Repo MA, Warrell RP Jr, *et al.* 1990; Distribution of trace levels of therapeutic gallium in bone as mapped by synchrotron x-ray microscopy. *Proc Natl Acad Sci U S A* **87**: 4149–4153.
- Boukhechba F, Balaguer T, Bouvet-Gerbettaz S *et al.* 2011; Fate of bone marrow stromal cells in a syngenic model of bone formation. *Tissue Eng Part A* **17**: 2267–2278.
- Bouletfour W, Boudiffa M, Wade-Gueye NM *et al.* 2014; Skeletal development of mice lacking bone sialoprotein (BSP) – impairment of long bone growth and progressive establishment of high trabecular bone mass. *PLoS One* **9**: e95144.
- Brackmann C, Zaborowska M, Sundberg J *et al.* 2012; In situ imaging of collagen synthesis by osteoprogenitor cells in microporous bacterial cellulose scaffolds. *Tissue Eng Part C Meth* **18**: 227–234.
- Brown WE, Chow LC. 1986; Effects of neutral salts in a bench-scale caries model. *J Dent Res* **65**: 1115–1120.
- Caetano-Lopes J, Nery AM, Canhao H *et al.* 2010; Chronic arthritis leads to disturbances in the bone collagen network. *Arthritis Res Ther* **12**: R9.
- Caetano-Lopes J, Nery AM, Henriques R *et al.* 2009; Chronic arthritis directly induces quantitative and qualitative bone disturbances leading to compromised

- biomechanical properties. *Clin Exp Rheumatol* **27**: 475–482.
- Chen J, Shapiro HS, Sodek J. 1992; Development expression of bone sialoprotein mRNA in rat mineralized connective tissues. *J Bone Miner Res* **7**: 987–997.
- Chen WC, Lin JH, Ju CP. 2003; Transmission electron microscopic study on setting mechanism of tetracalcium phosphate/dicalcium phosphate anhydrous-based calcium phosphate cement. *J Biomed Mater Res A* **64**: 664–671.
- Chitambar CR. 2010; Medical applications and toxicities of gallium compounds. *Int J Environ Res Public Health* **7**: 2337–2361.
- Chitambar CR. 2012; Gallium-containing anticancer compounds. *Future Med Chem* **4**: 1257–1272.
- Collery P, Keppler B, Madoulet C, et al. 2002; Gallium in cancer treatment. *Crit Rev Oncol Hematol* **42**: 283–296.
- Flausse A, Henrionnet C, Dossot M et al. 2013; Osteogenic differentiation of human bone marrow mesenchymal stem cells in hydrogel containing nacl powder. *J Biomed Mater Res A* **101**: 3211–3218.
- Franzen A, Hultenby K, Reinhold FP, et al. 2008; Altered osteoclast development and function in osteopontin deficient mice. *J Orthop Res* **26**: 721–728.
- Gelse K, Poschl E, Aigner T. 2003; Collagens – structure, function, and biosynthesis. *Adv Drug Deliv Rev* **55**: 1531–1546.
- Ginebra MP, Canal C, Espanol M et al. 2012; Calcium phosphate cements as drug delivery materials. *Adv Drug Deliv Rev* **64**: 1090–1110.
- Grzesik WJ, Robey PG. 1994; Bone matrix RGD glycoproteins: immunolocalization and interaction with human primary osteoblastic bone cells in vitro. *J Bone Miner Res* **9**: 487–496.
- Hall TJ, Chambers TJ. 1990; Gallium inhibits bone resorption by a direct effect on osteoclasts. *Bone Miner* **8**: 211–216.
- Hronik-Tupaj M, Rice WL, Cronin-Golomb M et al. 2011; Osteoblastic differentiation and stress response of human mesenchymal stem cells exposed to alternating current electric fields. *Biomed Eng Online* **10**: 9.
- Huang C, Ness VP, Yang X, et al. 2015; Spatiotemporal analyses of osteogenesis and angiogenesis via intravital imaging in cranial bone defect repair. *J Bone Miner Res* **30**: 1217–1230.
- Jenis LG, Waud CE, Stein GS, et al. 1993; Effect of gallium nitrate in vitro and in normal rats. *J Cell Biochem* **52**: 330–336.
- Koga T, Matsui Y, Asagiri M, et al. 2005; NFAT and Osterix cooperatively regulate bone formation. *Nat Med* **11**: 880–885.
- Komori T. 2006; Regulation of osteoblast differentiation by transcription factors. *J Cell Biochem* **99**: 1233–1239.
- Korbas M, Rokita E, Meyer-Klaucke W, et al. 2004; Bone tissue incorporates in vitro gallium with a local structure similar to gallium-doped brushite. *J Biol Inorg Chem* **9**: 67–76.
- Lee HS, Teng SW, Chen HC, et al. 2006; Imaging human bone marrow stem cell morphogenesis in polyglycolic acid scaffold by multiphoton microscopy. *Tissue Eng* **12**: 2835–2841.
- LeGeros RZ. 1982; Apatitic calcium phosphates: possible dental restorative materials. *J Dent Res* **61**: 343.
- LeGeros RZ. 1988; Calcium phosphate materials in restorative dentistry: a review. *Adv Dent Res* **2**: 164–180.
- Libicher M, Hillmeier J, Liegibel U, et al. 2006; Osseous integration of calcium phosphate in osteoporotic vertebral fractures after kyphoplasty: initial results from a clinical and experimental pilot study. *Osteoporos Int* **17**: 1208–1215.
- Liskova J, Babchenko O, Varga M, et al. 2015; Osteogenic cell differentiation on H-terminated and O-terminated nanocrystalline diamond films. *Int J Nanomedicine* **10**: 869–884.
- Liu H, Cui J, Sun J, et al. 2015; Histochemical evidence of zoledronate inhibiting c-src expression and interfering with CD44/OPN-mediated osteoclast adhesion in the tibiae of mice. *J Mol Histol* **46**: 313–323.
- Ma Z, Fu Q. 2010a; Comparison of the therapeutic effects of yeast-incorporated gallium with those of inorganic gallium on ovariectomized osteopenic rats. *Biol Trace Elem Res* **134**: 280–287.
- Ma Z, Fu Q. 2010b; Therapeutic effect of organic gallium on ovariectomized osteopenic rats by decreased serum minerals and increased bone mineral content. *Biol Trace Elem Res* **133**: 342–349.
- Mandelin J, Hukkanen M, Li TF, et al. 2006. Human osteoblasts produce cathepsin K. *Bone* **38**: 769–777.
- Masago Y, Hosoya A, Kawasaki K, et al. 2012; The molecular chaperone Hsp47 is essential for cartilage and endochondral bone formation. *J Cell Sci* **125**: 1118–1128.
- Mellier C, Fayon F, Boukhechba F, et al. 2015; Design and properties of novel gallium-doped injectable apatitic cements. *Acta Biomater* **24**: 322–332.
- Mellier C, Fayon F, Schnitzler V, et al. 2011; Characterization and properties of novel gallium-doped calcium phosphate ceramics. *Inorg Chem* **50**: 8252–8260.
- Merle B, Garnero P. 2012; The multiple facets of periostin in bone metabolism. *Osteoporos Int* **23**: 1199–1212.
- Nadiarnykh O, Plotnikov S, Mohler WA, et al. 2007; Second harmonic generation imaging microscopy studies of osteogenesis imperfecta. *J Biomed Opt* **12**: 051805.
- Niesvizky R. 2003; Gallium nitrate in multiple myeloma: prolonged survival in a cohort of patients with advanced-stage disease. *Semin Oncol* **30**: 20–24.
- Ooms EM, Wolke JG, van de Heuvel MT, et al. 2003a; Histological evaluation of the bone response to calcium phosphate cement implanted in cortical bone. *Biomaterials* **24**: 989–1000.
- Ooms EM, Wolke JG, van der Waerden JP, et al. 2003b; Use of injectable calcium-phosphate cement for the fixation of titanium implants: an experimental study in goats. *J Biomed Mater Res B Appl Biomater* **66**: 447–456.
- Paietta RC, Burger EL, Ferguson VL. 2013; Mineralization and collagen orientation throughout aging at the vertebral endplate in the human lumbar spine. *J Struct Biol* **184**: 310–320.
- Pei Y, Fu Q. 2011; Yeast-incorporated gallium promotes fracture healing by increasing callus bony area and improving trabecular microstructure on ovariectomized osteopenic rats. *Biol Trace Elem Res* **141**: 207–215.
- Reiser KM, Bratton C, Yankelevich DR, et al. 2007; Quantitative analysis of structural disorder in intervertebral disks using second harmonic generation imaging: comparison with morphometric analysis. *J Biomed Opt* **12**: 064019.
- Ribeiro N, Sousa SR, Brekken RA, et al. 2014; Role of SPARC in bone remodeling and cancer-related bone metastasis. *J Cell Biochem* **115**: 17–26.
- Rush SM. 2005; Bone graft substitutes: osteobiologics. *Clin Podiatr Med Surg* **22**: 619–630, viii.
- Stern LS, Matkovic V, Weisbrode SE, et al. 1994; The effects of gallium nitrate on osteopenia induced by ovariectomy and a low-calcium diet in rats. *Bone Miner* **25**: 59–69.
- Tang T, Ebacher V, Crompton P, et al. 2015; Shear deformation and fracture of human cortical bone. *Bone* **71**: 25–35.
- Tomita S, Kin A, Yazu M, et al. 2003; Biomechanical evaluation of kyphoplasty and vertebroplasty with calcium phosphate cement in a simulated osteoporotic compression fracture. *J Orthop Sci* **8**: 192–197.
- Verron E, Boulter JM, Scimeca JC. 2012a; Gallium as a potential candidate for treatment of osteoporosis. *Drug Discov Today* **17**: 1127–1132.
- Verron E, Gauthier O, Janvier P, et al. 2010a; In vivo bone augmentation in an osteoporotic environment using bisphosphonate-loaded calcium deficient apatite. *Biomaterials* **31**: 7776–7784.
- Verron E, Loubat A, Carle GF, et al. 2012b; Molecular effects of gallium on osteoclastic differentiation of mouse and human monocytes. *Biochem Pharmacol* **83**: 671–679.
- Verron E, Masson M, Khoshniat S, et al. 2010b; Gallium modulates osteoclastic bone resorption in vitro without affecting osteoblasts. *Br J Pharmacol* **159**: 1681–1692.
- Vielreicher M, Schurmann S, Detsch R, et al. 2013; Taking a deep look: modern microscopy technologies to optimize the design and functionality of biocompatible scaffolds for tissue engineering in regenerative medicine. *J R Soc Interface* **10**: 20130263.
- Wakley GK, Garand J, Brown D, et al. 1992; Effects of gallium on bone in the rat. *J Bone Miner Res* **7**: 11–19.
- Walsh MC, Choi Y. 2014; Biology of the RANKL-RANK-OPG system in immunity, bone, and beyond. *Front Immunol* **5**: 511.
- Warrell RP Jr, Bockman RS, Coonley CJ, et al. 1984; Gallium nitrate inhibits calcium resorption from bone and is effective treatment for cancer-related hypercalcemia. *J Clin Invest* **73**: 1487–1490.
- Warrell RP Jr, Bosco B, Weinerman S, et al. 1990; Gallium nitrate for advanced Paget disease of bone: effectiveness and dose-response analysis. *Ann Intern Med* **113**: 847–851.
- Warrell RP Jr, Israel R, Frisone M, et al. 1988; Gallium nitrate for acute treatment of cancer-related hypercalcemia. A randomized, double-blind comparison to calcitonin. *Ann Intern Med* **108**: 669–674.
- Welch RD, Zhang H, Bronson DG. 2003; Experimental tibial plateau fractures augmented with calcium phosphate cement or autologous bone graft. *J Bone Joint Surg Am* **85-A**: 222–231.